1

Fundamentals and Mechanisms of Vacuum Photoionization

Johannes Passig[1,2], *Ralf Zimmermann*[1,2], *and Thomas Fennel*[3]

[1] *Universität Rostock, Institut für Chemie, Analytical Chemistry and Joint Mass Spectrometry Centre (JMSC), Dr.-Lorenz-Weg 2, D-18059 Rostock, Germany*
[2] *Helmholtz Zentrum München, German Research Center for Environmental Health GmbH, Research Unit Comprehensive Molecular Analytics (CMA) and Joint Mass Spectrometry Centre, Gmunder Str. 37, D-81379 München, Germany*
[3] *Institute of Physics, University of Rostock, Albert-Einstein-Straße 23, D-18059 Rostock, Germany*

1.1 Preface

Within the past decades, the progress of laser-based light sources have opened various new research directions in the area of light-matter interactions. The ionization of free molecules with the purpose of their detection and mass-based identification may appear as an easy task in this context. However, experience has shown that already the simplest approach, the fragment-free ionization with single photons of sufficient energy, remains technically challenging. Beyond practical issues and applications, advanced photoionization techniques are an important field of study in spectroscopy and fundamental research. As an example, resonance-enhanced multiphoton ionization (REMPI, see chapters 2 and 4 of this book) bridges the gap between mass spectrometry (MS) and molecular spectroscopy, offering two-dimensional selectivity both in mass and in structure. In general, the absorption of a single photon by a molecule can lead to its ionization if the photon energy $E = h\nu = \hbar\omega$ is equal to or larger than the ionization potential I_p, where $h = 2\pi\hbar$ is the Planck constant, $\nu = c/\lambda$ is the photon frequency; λ is its wavelength, and c is the speed of light. It is worth to have a look on the typical energy- and timescales that constitute the framework of photoionization processes as illustrated in Figure 1.1. Electron motion and electronic transitions are much faster than atomic motion on molecular scales. This is the basis for important approximations in atom and molecular physics and spectroscopy. Current tabletop laser systems are available from infrared (IR) to ultraviolet (UV), with ultrashort pulses that allow to analyze molecular processes on their physical or natural timescale. Laser intensities for (multi-) photoionization MS span the range from the onset of REMPI ($\approx 10^6$ W/cm^2) to the strong field regime ($> 10^{14}$ W/cm^2) and beyond for complex laser sources. Tuning the photon energy remains rather complicated both for lamp- and laser-based sources. However, the latter implicates further parameters as phase

Photoionization and Photo-Induced Processes in Mass Spectrometry: Fundamentals and Applications, First Edition. Edited by Ralf Zimmermann and Luke Hanley.

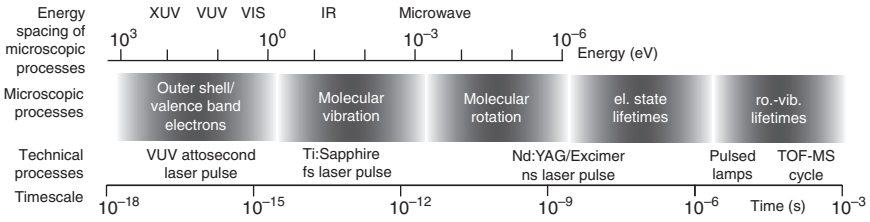

Figure 1.1 Typical energy- and timescales of processes related to photoionization.

or chirp, which are linked to the coherence of laser pulses and are likely to increase the selectivity in future applications.

When dealing with photoionization MS, natural questions about the underlying mechanisms of photoabsorption and photoionization arise at some point. A brief standard answer might be as follows: Assume two eigenstates of a molecular system with different electronic charge distributions. Upon excitation from the lower to the upper state and assuming a single active electron, the system corresponds to a quantum superposition of those two states and the electronic charge oscillates with an amplitude that reflects the transition dipole moment. Now, assume a light field acting on it. Thus, the electron "feels" an oscillating electric field from the light. If the frequencies, direction (polarization), and shape of charge distribution associated with a transition, match the light field and the molecule couple and the electron will be resonantly driven into the excited state while the light wave is damped. If the excited state is a continuum state, the electron is ejected.

This description provides a basic, phenomenological understanding, and some readers consider now to skip the following pages with complicated formulas. However, it is a problematic simplification, mixing different concepts and principles. The following section will provide an introductory survey on photoabsorption, being the physical basics of photoionization. The scope is not to treat the full complexity of optics and spectroscopy but to give an outline of some fundamental principles being useful for its conceptual understanding.

1.2 Light

The physics of classical light propagation, optics, and electromagnetism is based on the Maxwell equations, a set of partial differential equations that describe the behavior of the electric field $\mathbf{E}(\mathbf{r}, t)$ and the magnetic field $\mathbf{B}(\mathbf{r}, t)$ with respect to charges ρ and currents $\mathbf{j}$:

$$\nabla \cdot \mathbf{E}(\mathbf{r}, t) = \rho(\mathbf{r}, t)/\epsilon_0 \tag{1.1}$$

$$\nabla \cdot \mathbf{B}(\mathbf{r}, t) = 0 \tag{1.2}$$

$$\nabla \times \mathbf{E}(\mathbf{r}, t) = -\frac{\partial}{\partial t}\mathbf{B}(\mathbf{r}, t) \tag{1.3}$$

$$\nabla \times \mathbf{B}(\mathbf{r}, t) = \mu_0 \mathbf{j} + \mu_0 \epsilon_0 \frac{\partial}{\partial t}\mathbf{E}(\mathbf{r}, t) \tag{1.4}$$

The divergence $\nabla \cdot \mathbf{F} = \frac{\partial F_x}{\partial x} + \frac{\partial F_y}{\partial y} + \frac{\partial F_z}{\partial z}$ of a vector field $\mathbf{F}$ produces a scalar field, giving the quantity of $\mathbf{F}$'s source (outward flux) at each point. An expanding vector field (e.g. heated air) yields positive divergence values, whereas a contracting one (e.g. cooled air) yields negative values. The curl $\nabla \times \mathbf{F}$ yields a vector field that describes the infinitesimal rotation of $\mathbf{F}$ at each point, e.g. the circulation density of a flow.

Fundamental properties of light can be derived from this set of equations. Later, we will have to construct a Hamiltonian to describe photoabsorption. Because it represents the system total energy in quantum mechanics, it will be natural to use potentials rather than fields. In electrostatics, the field is related to the electrostatic potential through

$$\mathbf{E}(\mathbf{r}) = -\nabla\Phi(\mathbf{r}) \tag{1.5}$$

However, for a field that varies in time and in space, the electrodynamic potential must be expressed in terms of both the time-dependent scalar potential $\phi(\mathbf{r}, t)$ and the vector potential $\mathbf{A}(\mathbf{r}, t)$. According to Eq. (1.5), the fields $\mathbf{E}(\mathbf{r}, t)$ and $\mathbf{B}(\mathbf{r}, t)$ can be expressed as

$$\mathbf{E}(\mathbf{r}, t) = -\nabla\phi(\mathbf{r}, t) - \frac{\partial}{\partial t}\mathbf{A}(\mathbf{r}, t) \tag{1.6}$$

$$\mathbf{B}(\mathbf{r}, t) = \nabla \times \mathbf{A}(\mathbf{r}, t) \tag{1.7}$$

This definition automatically fulfills Eqs. (1.2) and (1.3). Furthermore, it allows a transformation of the potentials into Coulomb gauge, where $\mathbf{A}$ is divergence-free ($\nabla \cdot \mathbf{A} = 0$), whereas the physical observables $\mathbf{E}(\mathbf{r}, t)$ and $\mathbf{B}(\mathbf{r}, t)$ remain unchanged (not shown here). In Coulomb gauge, the scalar potential is identical with the Coulomb potential, yielding $\phi = -\rho/\varepsilon_0$ for Eq. (1.1). Furthermore, if charges and currents are absent, only Eq. (1.4) determines $\mathbf{A}$ (and thus $\mathbf{E}$ and $\mathbf{B}$) in the following form of a wave equation:

$$\nabla^2\mathbf{A}(\mathbf{r}, t) - \frac{1}{c^2}\frac{\partial^2}{\partial t^2}\mathbf{A}(\mathbf{r}, t) = 0 \text{ with } c^2 = \frac{1}{\sqrt{\mu_0\epsilon_0}} \tag{1.8}$$

Solutions are linearly polarized plane waves

$$\mathbf{A}(\mathbf{r}, t) = \frac{1}{2}\tilde{A}\varepsilon e^{i(\mathbf{k}\cdot\mathbf{r}-\omega t)+\delta} + c.c. = \tilde{A}\varepsilon\cos(\mathbf{k}\cdot\mathbf{r} - \omega t + \delta) \tag{1.9}$$

with amplitude $\tilde{A}$, polarization vector ε, imaginary unit i, wave vector k, angular frequency ω, and phase offset δ. Several primary properties of light can now be derived, such as the dispersion relation $\omega = ck$ when inserting the solution into Eq. (1.8) or the orthogonality of wave and polarization vectors $\mathbf{k} \cdot \varepsilon = 0$ that directly results from the gauge condition $\nabla \cdot \mathbf{A} = 0$. The electric and magnetic fields follow as plane waves, mutually orthogonal also with the propagation direction due to the vector product $\mathbf{k} \times \varepsilon$

$$\mathbf{E}(\mathbf{r}, t) = \tilde{E}\varepsilon \ \sin(\mathbf{k}\cdot\mathbf{r} - \omega t + \delta) \tag{1.10}$$

$$\mathbf{B}(\mathbf{r}, t) = \frac{\tilde{E}}{\omega}(\mathbf{k}\times\varepsilon) \ \sin(\mathbf{k}\cdot\mathbf{r} - \omega t + \delta) \tag{1.11}$$

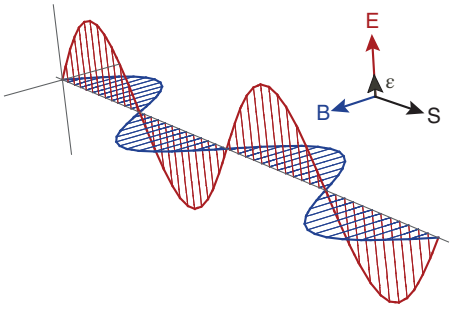

Figure 1.2 Illustration of a linearly polarized light wave as a solution of Eq. (1.8) with mutually orthogonal electric field **E**, magnetic field **B**, and propagation as well as energy transport in direction of the Poynting vector **S**. Polarization vector ε. Eq. (1.16).

with $\tilde{E} = -\omega\tilde{A}$. A key parameter for many applications is the light intensity, respectively the photon density. They follow from the (instantaneous) energy density of the electromagnetic field

$$u = \frac{1}{2}\left[\epsilon_0|\mathbf{E}\ |^2 + \frac{1}{\mu_0}|\mathbf{B}\ |^2\right] = \epsilon_0\tilde{E}^2\ \sin^2(\mathbf{k}\cdot\mathbf{r} - \omega t + \delta) \tag{1.12}$$

The rapid oscillations can be averaged as $\langle\sin^2\rangle = 1/2$, yielding the mean energy that can alternatively be expressed in terms of the photon density $n_{\mathrm{ph}} = dN_{\mathrm{ph}}/dV$

$$\langle u\rangle = \frac{1}{2}\epsilon_0\tilde{E}^2 = n_{\mathrm{ph}}\hbar\omega \tag{1.13}$$

Energy transport by light propagation is characterized using the Poynting vector

$$\mathbf{S} = \frac{1}{\mu_0}\mathbf{E}\times\mathbf{B} = \epsilon_0 c\frac{\mathbf{k}}{k}\tilde{E}^2\sin^2(\mathbf{k}\cdot\mathbf{r} - \omega t + \delta) \tag{1.14}$$

The absolute value of its time-average $|\langle\mathbf{S}\rangle|$ is the commonly used light intensity (unit $\mathrm{W/m^2}$)

$$I = \frac{1}{2}\epsilon_0 c\tilde{E}^2 = cn_{\mathrm{ph}}\hbar\omega \tag{1.15}$$

Note that the intensity I is proportional to the square of the field (amplitude) $\tilde{E}^2$. The photon flux φ (unit photons/($\mathrm{m^2\ s}$)) can be expressed in terms of the intensity and photon energy or via the photon density n_{ph} and the speed of light c.

$$\varphi = \frac{I}{\hbar\omega} = n_{\mathrm{ph}}c \tag{1.16}$$

Next, the general cross section σ is a coefficient of proportionality between the rate W of an induced transition and the photon flux

$$W = \varphi\sigma(\omega) \tag{1.17}$$

with unit megabarn ($1\ \mathrm{Mb} = 10^{-18}\ \mathrm{cm^2}$).

1.3 Photoabsorption

In classical physics, light absorption is interpreted as damping of a periodic electric field by dipoles oscillating with opposite phase at the same frequency. This basic picture provides a descriptive explanation of optical properties and some fundamental interactions. However, a description of the photoionization of atoms and molecules is only possible in a quantum mechanical context. Upon light absorption, a system undergoes a transition from an initial state to a final state of higher energy with energy difference $\hbar\omega$. Because the charge distributions of the states differ, their coherent superposition results in an oscillating dipole that can couple to the light field under appropriate conditions.

1.3.1 Transitions in First Order Perturbation Theory

Some essential principles needed for the quantum mechanical description are the representation of (electronic) states by wavefunctions $\Psi(\mathbf{r}, t)$ and physical observables by their corresponding operators.

In quantum mechanics, the state $|\psi\rangle$ of a system can be described by a complex wavefunction $\psi(\mathbf{r}, t)$ in coordinate space representation. A physical observable is represented by a linear operator $\hat{O}$ acting on the state producing a new vector $\hat{O}|\psi\rangle = |\psi^*\rangle$. If $|\psi\rangle$ is an eigenstate of an observable, the equation $\hat{O}|\psi\rangle = a \cdot |\psi\rangle$ yields the associated eigenvalues a, corresponding to the value of the observable in that eigenstate. Eigenvalues a can be continuous (e.g. for the position operator $\hat{\mathbf{r}}$) or discrete as for the angular momentum operator and thus be expressed by quantum numbers.

The time evolution of a physical system is described by solutions of the time-dependent Schrödinger equation (TDSE) in its general form

$$i\hbar \frac{\partial}{\partial t} \Psi(\mathbf{r}, t) = \hat{H} \Psi(\mathbf{r}, t) \tag{1.18}$$

where i is the imaginary unit, $\hbar$ is the Planck constant, and $\hat{H}$ is the Hamiltonian operator representing the system's total energy.

An analytical solution is only possible for very simple systems, such as the hydrogen atom. Already the presence of an external field or a second electron renders closed and analytical solutions impossible. Typically, several approximations allow for the treatment of a molecular system with minimum deficiency, depending on the framework of the scientific problem. Common approaches for atom-light interactions apply the single active electron approximation (SAE) that treats a single interacting electron in an effective potential (e.g. Hartree-Fock) resembling both the atomic core and the (mean) electron-electron interactions.

In general, photoionization can be understood as one of several possible secondary processes upon photoabsorption. For the weak field regime[1], which applies even beyond typical REMPI intensities of about 10^7 W/cm^2, the description of photoabsorption is convenient via perturbation theory. Its basic concept is the partition of the Hamiltonian $\hat{H}$ into the calculable Hamiltonian $\hat{H}_0$ of a simplified and known system (which may be artificial) and an additional Hamiltonian $\hat{H}'$ representing the weak disturbance to the system that is quantified using approximate methods.

1.3.2 Perturbation Theory

For our basic considerations of photoabsorption via electronic states, we describe an atom by a single electron of charge $q = e$ and mass $m_e = m$ in a Coulomb potential $V_C = -Ze^2/4\pi\epsilon_0 r$, which represents a stationary nucleus. The vector potential remains classical. Considering that in Coulomb gauge, the scalar potential equals V_C (see Section 1.2), the Hamiltonian of the electron splits into a stationary part of the undisturbed atom $\hat{H}_0$ and a time-dependent part $\hat{H}_{\text{int}}(t)$ for the interaction with the light field. $\hat{H}_{\text{int}}(t)$ can be derived from the classical Hamiltonian for a charged particle in a radiation field (not shown here)

$$\hat{H} = \underbrace{-\frac{\hbar^2}{2m}\boldsymbol{\nabla}^2 + V_c}_{\hat{H}_0} \underbrace{- i\hbar\frac{e}{m}\mathbf{A}\cdot\boldsymbol{\nabla} + \frac{q^2}{2m}A^2}_{\hat{H}_{\text{int}}(t)} \tag{1.19}$$

For the first term $\hat{H}_0$, the analogy to the corresponding classical total energy $E_{\text{kin}} + V = \frac{p^2}{2m} + V$ is clearly visible, if the notation of the momentum operator $\hat{p} = -i\hbar\frac{\partial}{\partial x}$ is considered.

For moderate field strengths ($I \ll 10^{15}$ W/cm^2), the last term is small compared to the cross term, which simplifies the interaction Hamiltonian H_{int} to

$$H_{\text{int}} \approx -i\hbar\frac{e}{m}\mathbf{A}\cdot\boldsymbol{\nabla} \tag{1.20}$$

According to perturbation theory, the wavefunction $\Psi(\mathbf{r}, t)$ can be expressed as a linear combination of unperturbated eigenstates $\Psi(\mathbf{r})$ of the stationary Schrödinger equation (time-independent Hamiltonian) $H_0\Psi_j(\mathbf{r}) = E_j\Psi_j(\mathbf{r})$ with the time-dependent coefficients $c_j(t)$

$$\Psi(\mathbf{r}, t) = \sum_j c_j(t)\Psi_j(\mathbf{r})e^{-iE_jt/\hbar} \tag{1.21}$$

1 The term "weak disturbance" indicates an important limitation for laser-based photoionization: The external laser field, treated as perturbation, has to be small against the inner atomic forces. Thus, laser intensities exceeding 10^{12} W/cm^2 and molecular interactions induced thereby are often referred to as "nonperturbative" (Baumert and Gerber 1997), while typical intensities for single-photon ionization (SPI) and REMPI applications are below 10^8 W/cm^2.

Inserting in the TDSE (Eq. (1.18)) yields

$$\sum_j (i\hbar \frac{d}{dt} c_j(t) + E_j) e^{-iE_j t/\hbar} |\Psi_j\rangle = \sum_k (E_k + H_{\text{int}}(t)) c_k(t) e^{-iE_k t/\hbar} |\Psi_k\rangle \tag{1.22}$$

The "ket" vector $|\Psi\rangle$ represents the state that is associated with the wavefunction $\Psi(r,t)$. With the corresponding "bra" vector $\langle\Psi|$, that corresponds to the complex conjugated wavefunction $\Psi^*(r,t)$ in coordinate space, and with the inner product $\langle\Psi|\Psi\rangle = \int \Psi^*\Psi dr$ and the operator H acting on $|\Psi\rangle$, we can express the expectation value of the observable (here energy) represented by operator H in the state $|\Psi\rangle$ by $\langle\Psi|H|\Psi\rangle$.

Considering the orthogonality of the eigenstates, the result is a set of coupled equations for the time evolution of coefficients $c_j(t)$ with the transition frequency $\omega_{jk} = (E_j - E_k)/\hbar$:

$$\frac{d}{dt} c_j(t) = \frac{1}{i\hbar} \sum_k \underbrace{\langle \Psi_j | H_{\text{int}}(t) | \Psi_k \rangle}_{H^{jk}_{\text{int}}(t)} c_k(t) e^{i\omega_{jk} t} \tag{1.23}$$

Assuming a two-level system with initial state $|\Psi_a\rangle$ and the interaction Hamiltonian (1.20), the coefficient $c_b(t)$ for the state $|\Psi_b\rangle$ can be expressed in the following form.

$$c_b(t) = \frac{1}{i\hbar} \int_0^t H^{ba}_{\text{int}}(t') e^{i\omega_{ba} t'} dt' = -\frac{e}{m} \int_0^t \langle \Psi_b | \mathbf{A} \cdot \boldsymbol{\nabla} | \Psi_a \rangle e^{i\omega_{ba} t'} dt' \tag{1.24}$$

Applying the vector potential $\mathbf{A}$ for the electromagnetic field representing the classic description of light (Section 1.2)

$$\mathbf{A}(\mathbf{r},t) = \tilde{A}\varepsilon \cos(\mathbf{kr} - \omega t + \delta) = \frac{1}{2}\tilde{A}\varepsilon [e^{i(\mathbf{kr}-\omega t+\delta)} + e^{-i(\mathbf{kr}-\omega t+\delta)}] \tag{1.25}$$

yields the time-dependent amplitude of state $|\Psi_b\rangle$ in first-order perturbation theory

$$\begin{aligned} c_b(t) = -\tfrac{e}{2m}\tilde{A}[e^{i\delta} \underbrace{\langle \Psi_b | e^{i\mathbf{kr}} \varepsilon \cdot \boldsymbol{\nabla} | \Psi_a \rangle}_{M_{ba}(\omega)} \int_0^t e^{i(\omega_{ba}-\omega)t'} dt' \\ + e^{-i\delta} \langle \Psi_b | e^{-i\mathbf{kr}} \varepsilon \cdot \boldsymbol{\nabla} | \Psi_a \rangle \int_0^t e^{i(\omega_{ba}+\omega)t'} dt'] \end{aligned} \tag{1.26}$$

The first integral describes the absorption of a photon. Because the complex e-function is periodic with mean value zero for $\omega_{ba} \neq \omega$, it contributes only for $\omega_{ba} = \omega \Rightarrow E_b = E_a + \hbar\omega$ while the second integral corresponds to the photon emission if $\omega_{ba} = -\omega \Rightarrow E_b = E_a - \hbar\omega$.

1.3.3 Absorption

The matrix element associated with the perturbation $M_{ba}(\omega) = \langle \Psi_b | e^{i\mathbf{kr}} \varepsilon \cdot \boldsymbol{\nabla} | \Psi_a \rangle$ in Eq. (1.26) connects the initial state with the final state and thus determines the system interaction strength with the light. Before its further evaluation, we

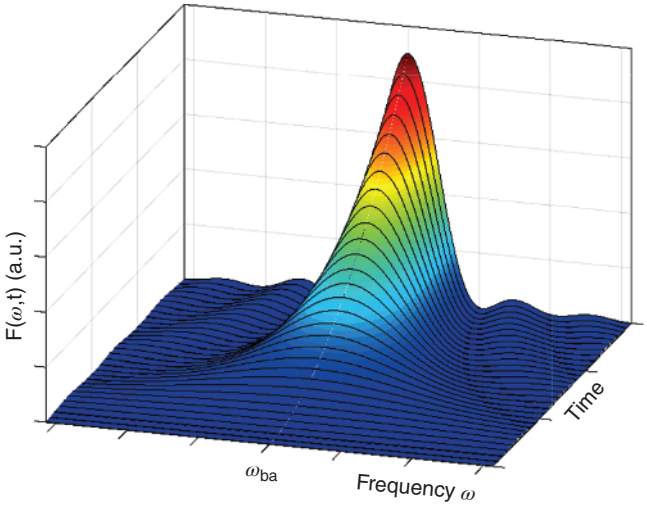

Figure 1.3 Behavior of the function $F(\omega, t)$ (Eq. (1.28)) that determines the time evolution of the transition when the field and the system are in resonance. If the light frequency ω equals the transition frequency ω_{ba} of the states $|\Psi_a\rangle$ and $|\Psi_b\rangle$, the function peaks increasingly and transforms into the δ-function in the long-time limit.

derive corresponding transition rates and cross sections. During absorption, the occupation probability $c_b(t)$ of the state $|\Psi_b\rangle$ increases with time, which can be expressed through integration of the first term in Eq. (1.26)

$$|c_b(t)|^2 = \left| -\frac{e}{2mi}\tilde{A}e^{i\delta}M_{ba}(\omega)\frac{e^{i(\omega_{ba}-\omega)t}-1}{\omega_{ba}-\omega}\right|^2 = \frac{1}{2}\frac{e^2}{m^2}\tilde{A}^2|M_{ab}(\omega)|^2F(t,\tilde{\omega}) \tag{1.27}$$

with

$$F(t,\tilde{\omega}) = \frac{1-\cos(\tilde{\omega}t)}{\tilde{\omega}^2} \tag{1.28}$$

and the frequency offset $\tilde{\omega} = \omega - \omega_{ba}$. As illustrated in Figure 1.3, the transition probability increases sharply with time according to function (1.28) when the external field and the system are in *resonance*, hence $\omega = \omega_{ba}$.

Equations (1.27) and (1.28) describe the evolution of the occupation probability of state $|\Psi_b\rangle$ with time and thus characterize the rate with which transitions appears. During excitation, the states $|\Psi_a\rangle$ and $|\Psi_b\rangle$ form a coherent superposition and the associated dipole oscillates with the transition frequency.

For timescales longer than a cycle ($t \gg 2\pi/|\omega_{ba}|$), Eq. (1.28) changes to a delta function $F(t,\tilde{\omega}) \Rightarrow \pi t\delta(\omega - \omega_{ba})$ (note: $\delta(\tilde{\omega}) \to \infty$ for $\tilde{\omega} \to 0$). Furthermore, we express the amplitude $\tilde{A}$ of the vector potential by the light intensity I (compare Eq. (1.15)).

$$\tilde{A}^2 = \frac{2I}{\epsilon_0 c\omega^2} \tag{1.29}$$

and find the frequency-dependent absorption rate

$$W_{ba}(\omega) = \frac{\pi e^2}{\epsilon_0 \mathrm{cm}^2} \frac{I}{\omega^2} |M_{ba}(\omega)|^2 \delta(\omega - \omega_{ba}) \tag{1.30}$$

So far, we assumed perfectly monochromatic light corresponding to an infinite plane wave. However, the intensity of realistic light has components covering at least a narrow band over a frequency range $I(\omega) = dI/d\omega$; thus, the total absorption rate has to be integrated over the entire spectrum

$$W_{ba} = \int W_{ba}(\omega) I(\omega) d\omega \tag{1.31}$$

In the long-time limit, only the value at ω_{ba} contributes to W_{ba} by nature of the delta function

$$W_{ba} = \frac{\pi e^2}{\epsilon_0 \mathrm{cm}^2} \frac{I(\omega_{ba})}{\omega_{ba}^2} |M_{ba}(\omega_{ba})|^2 \tag{1.32}$$

To express the associated cross section, we use Eq. (1.17)

$$\hbar \omega_{ba} W_{ba} = I(\omega_{ba}) \sigma_{ba} \tag{1.33}$$

which yields the absorption cross section for the spectral intensity associated with the considered transition. Note that the unit of the cross section is therefore area times frequency.

$$\sigma_{ba} = \frac{\pi \hbar}{\epsilon_0 c} \frac{e^2}{m^2} \frac{1}{\omega_{ba}} |M_{ba}(\omega_{ba})|^2 \tag{1.34}$$

Of note, the integration (1.31) assumes a sum of incoherent spectral components. The treatment of absorption from coherent and ultrashort laser pulses has to consider the explicit pulse waveform.

Molecules typically have numerous states in a small energy interval that contributes to the absorption. Hence, the transition probability into this band is the sum of all transition probabilities matching the frequency of the incident light. The number of states in an energy range between E_b and $E_b + dE$ can be expressed as $\rho(E_b)dE$, where $\rho(E_b)$ is called the density of states. Assuming that the matrix elements for transitions into such a band of states are comparable, Fermi's golden rule can be derived via spectral integration of the transition rates (not shown).

$$W_{ba} = \frac{2\pi}{\hbar} \rho(E_b) |M_{ba}|^2 \tag{1.35}$$

Thus, to calculate the transition rate into a band, multiply the square of the matrix element by the density of states of the involved bands.

1.3.4 Dipole Approximation

So far, the matrix elements are dependent on the wavelength and direction of the light wave (photon) via the $e^{i\mathbf{kr}}$ term. For interactions with visible, (V)UV, and IR (but not X-ray) radiation, the wavelength is much larger than the atomic length scale; hence, the system "feels" an oscillating dipole field. As a consequence, the wave vector dependence of the vector potential can be neglected, according to

$e^{i\mathbf{kr}} \approx 1$ for $\lambda \to \infty; \mathbf{k} \to 0$. In this so-called *dipole approximation*, the vector potential $\mathbf{A}(\mathbf{r}, t) \to \mathbf{A}(t)$ describing the light field becomes spatially homogenous and, as a consequence, the magnetic field $\mathbf{B} = \nabla \times \mathbf{A}$ vanishes. Descriptively, the electron velocity $\mathbf{v}_e$ is low enough to neglect both the magnetic Lorentz force $e(\mathbf{v}_e \times \mathbf{B})$ and the relativistic effects that arise if the electron is driven at very high intensities ($> 10^{16}$ W/cm^2), predominantly for long wavelengths. The matrix elements M^D_{ba} can now expressed by the dipole matrix element in the so-called length form via the transition dipole moment $\mathbf{D}_{ba} = -e\mathbf{r}_{ba}$ containing spatial coordinates $(\hat{x}, \hat{y}, \hat{z})$ of the position operator $\mathbf{r}$

$$M^D_{ba} = \frac{m\omega_{ba}}{\hbar e}\varepsilon \cdot (-e\langle \Psi_b|\mathbf{r}|\Psi_a\rangle) = \frac{m\omega_{ba}}{\hbar e}\varepsilon \cdot \mathbf{D}_{ba} \tag{1.36}$$

Thus, the matrix element of the interaction Hamiltonian, representing the expectation value of its energy spectrum, is now related to the much more descriptive dipole matrix element $\mathbf{D}_{ba}$, which represents the charge distribution within the wavefunction.

The dipole matrix element $\mathbf{D}_{ba}$ (and also M_{ba}) determines the interaction strength between light and the atom or molecule. Its scalar part describes the change of charge distribution during transition from $|\Psi_a\rangle$ to $|\Psi_b\rangle$ that determines the transition probability. The vector part demands projection of the light field onto the dipole moment, i.e. it defines the required light polarization.

The corresponding absorption rate can be derived to

$$W^D_{ba} = \frac{\pi}{3\epsilon_0 c\hbar^2} I(\omega_{ba})|\mathbf{D}_{ba}|^2 = \frac{\pi e^2}{3\epsilon_0 c\hbar^2} I(\omega_{ba})|\mathbf{r}_{ba}|^2 \tag{1.37}$$

If the dipole matrix element is zero, the transition is so-called *dipole-forbidden*. However, such transitions are often observed because they may be allowed as (weaker) magnetic dipole or electric quadrupole transitions. Commonly used in spectroscopy to describe the absorption strength is the dimensionless *oscillator strength* f_{ij} of a transition between states i and j

$$f_{ij} = \frac{2m_e\omega_{ij}}{3\hbar}|\mathbf{r}_{ij}|^2 \tag{1.38}$$

Oscillator strength values are between 0 and 1. Typical values are shown in Table 1.2.

An interesting application of transition rates is related to the famous *Einstein coefficients*. Therefore, the Boltzmann distribution is applied to the level population of an ensemble of atoms in equilibrium and the Planck distribution to the photon field. An interesting finding in the context of VUV sources is that spontaneous emission increases relative to stimulated emission as the cube of light frequency. Hence, population inversion, which is a basis of laser sources, is difficult to generate and maintain in highly excited systems. Instead of cooperating in a stimulated emission process, the excited populations randomly loose energy via spontaneous emission.

1.3.5 Selection Rules

To calculate absorption rates, the corresponding matrix elements have to be evaluated by spatial integration over the corresponding wave functions $\langle \Psi_b | \mathbf{r} | \Psi_a \rangle = \int \Psi_b \mathbf{r} \, \Psi_a d\mathbf{r}$ in Eq. (1.36). If the integral vanishes, a transition does not occur (with the exception of higher order transitions), which is called dipole-forbidden. In particular, this is the case if the function $\Psi_b \mathbf{r} \, \Psi_a$ is antisymmetric, and thus, its integral over space yields zero. This can often be determined by analysis of the wavefunction symmetry without explicit calculation of the integral. For example, dipole transitions (e.g. $|s\rangle \rightarrow |s\rangle$) are not allowed for the hydrogen atom. The symmetry behavior is reflected by the parity selection rule (ref. third column in Table 1.1). Using quantum numbers to term the states, further selection rules for dipole transitions can be derived by evaluation of zero and nonzero matrix elements, as $\Delta l = \pm 1$ and $\Delta m = 0, \pm 1$, where l is the angular momentum quantum number and m is the magnetic quantum number in a one-electron system. Descriptively, these rules reflect conservation of angular momentum because the spin of the absorbed photon contributes to the system's angular momentum $\mathbf{L}$. The z-component of $\mathbf{L}$ is associated with the electrons' magnetic moment, which couples to the photon spin, thus yielding $\Delta m = 0$ in the case of linear polarization and $\Delta m = \pm 1$ for circularly polarized light. For multielectron systems, the total angular and orbital momentum as well as the total spin is evaluated, and coupling schemes of angular momentum sources are considered. In realistic systems, especially molecules, several dipole-forbidden transitions can nevertheless be observed. For example, the dipole-forbidden transitions may be allowed as multipole transitions. Typically, the rate drops down by three orders of magnitude from one multipole to the next, see Table 1.2.

1.3.6 Electronic Line Width and Lifetime

So far, we assumed that the states have sharp eigen energies and can be described via time-dependent wavefunctions of the form $\psi e^{-iEt/\hbar}$ (ref. Figure 1.4a,d). Suppose a state that is exponentially decaying in amplitude as the system changes to another state (Figure 1.4b). The decaying function corresponds

Table 1.1 Dipole selection rules for electronic transitions in a Hydrogen-like atom. $J = L + S$ is the total angular momentum, L is the total orbital momentum quantum number, S is the total spin quantum number, M_J is the total magnetic quantum number, and π is the parity.

Rigorous			LS coupling		Intermediate coupling
$\Delta J = 0, \pm 1$ ($J = 0 \not\leftrightarrow 0$)	$\Delta M_J = 0, \pm 1$	$\pi_b = -\pi_a$	[a] $\Delta l = \pm 1$	[b] if $\Delta S = 0$: $\Delta L = 0, \pm 1$, ($L = 0 \not\leftrightarrow 0$)	[c] if $\Delta S = \pm 1$: $\Delta L = 0, \pm 1, \pm 2$

a) Rigorous for one-electron systems.
b) Small atoms with low LS-coupling.
c) Heavier atoms with transitions between several multiplet states.

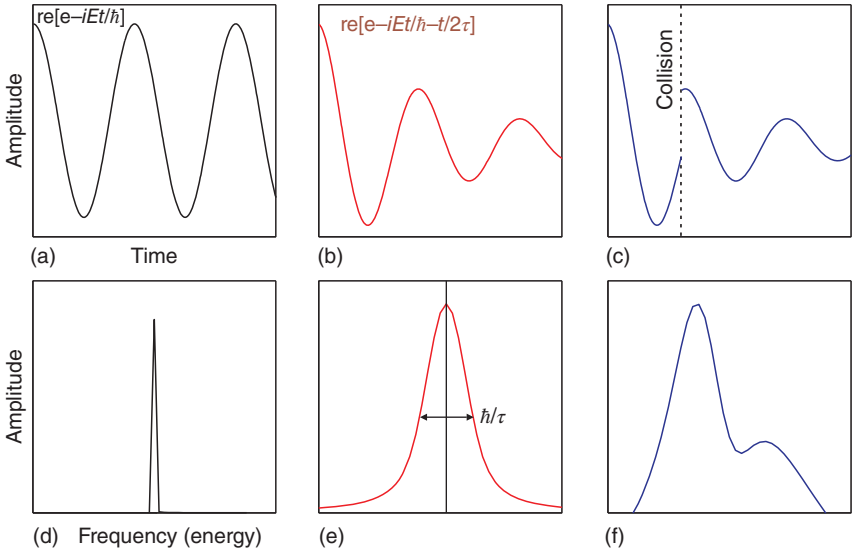

Figure 1.4 Schematic wavefunctions (top) and their spectra (bottom). (a, d) Stationary state. (b, e) Decaying state and resulting Lorentzian line profile. (c, f) Collision-induced phase distortion and its resulting spectrum (fast Fourier transformed).

to a superposition of oscillations whose frequencies can be Fourier analyzed according to

$$e^{-iEt/\hbar - t/\tau} = \int g(E')e^{-iE't/\hbar}dE' \text{ with } g(E') = \frac{1}{\pi}\frac{(\hbar/\tau)}{(E-E')^2 + (\hbar/\tau)^2} \tag{1.39}$$

where τ is the time constant of the decay. Therefore, the decaying dipole oscillation is associated with a finite energy range. The width at half height of the Lorentzian function $g(E')$ is $\hbar/\tau$ and called *natural line width* (Figure 1.4e). Considering that the state to which the transition appears may also have a finite lifetime τ_b, the line width is given by

$$\delta E = \hbar\left(\frac{1}{\tau_b} + \frac{1}{\tau_a}\right) \tag{1.40}$$

Hence, the shorter the state lifetime, the less precise its energy and vice versa. This concept is particularly important for REMPI (see Chapter 2), where ionization rates depend on the energy match between the photon and possible intermediate states as well as the photon density. It further gives rise to the concept of virtual states of uncertain energy, which may be employed at high photon densities.

Measured line widths are typically much larger, which can be attributed to the other origins of broadening. First, collisions with other atoms may lead to (radiative or nonradiative) transitions and randomize the phase of emitted radiation (ref. Fig. 1.4c,f). Both reduces the effective lifetime of the state and leads to the (pressure-dependent) *collision broadening* of the Lorentzian line profile. Secondary, the relative motion of atoms results in frequency shift. Thus, the so-called *Doppler broadening* increases with temperature and decreases

with atomic mass and produces a Gaussian profile, which convolves with the Lorentzian profile.

1.3.7 Electronic Transitions of Molecules

So far, we treated light absorption using a simple model system undergoing electronic transitions. However, real electronic spectra of molecules are highly complex. This cannot be comprehended by single-electron transitions in a static potential model as the nucleic motion is completely neglected. Indeed, any electronic transition changes a real system's charge distribution inducing vibration of the nuclei, which, in turn, changes the rotational state. Moreover, full understanding of the molecule response implies consideration of all possible sources of angular momentum and their coupling scheme. Note that for photoionization, REMPI cross sections are a consequence of the actual electronic structure. In direct SPI, the outgoing states are continuum states, being less restricted.

Corresponding to atoms, selection rules arise from the conservation of total angular momentum and the total parity changes in dipole transitions, refer Table 1.2. Initial estimates on cross sections can be derived from typical oscillator strength values and respective transition probabilities, as summarized in Table 1.2 and indicated by exemplary absorption spectrum of benzene (Figure 1.5).

Several schemes allow for (at least qualitative) indications on the molecules' electronic spectra and transition probabilities. Hund's rules describe how the four sources of angular momentum (electron orbital angular momenta **L**, rotation of nuclear framework **O**, and spin of electrons **S** and nucleus **I**), are coupled (in a diatomic molecule). Any electronic transition changes the charge distribution. The nuclei readjust to these forces causing vibration. Consequently, electronic transitions in molecules are accompanied with vibrational transitions, giving rise to the term *vibronic* transitions that have many lines in the absorption spectra. Of note, nuclear rearrangement is much slower than electronic transitions, see also Figure 1.1. This is the basis for the Franck–Condon principle that makes statements on the most probable vibronic (electronic + induced vibrational) transitions, see Figure 1.6. Electronic excitation is virtually instantaneous before the nuclei can readjust to the distance r_B and must therefore be drawn as a "vertical" transition (blue arrow). From the numerous vibrational states of the upper electronic level, the one with the greatest overlap with the original state vibrational wavefunction is occupied.

Table 1.2 Typical oscillator strengths for transitions according to the selection rules

	Oscillator strength *f*
Electric dipole allowed	$\lesssim 1$
Parity forbidden	10^{-1}
Magnetic dipole allowed	10^{-5}
Electric quadrupole allowed	10^{-5}
Spin forbidden	10^{-5}

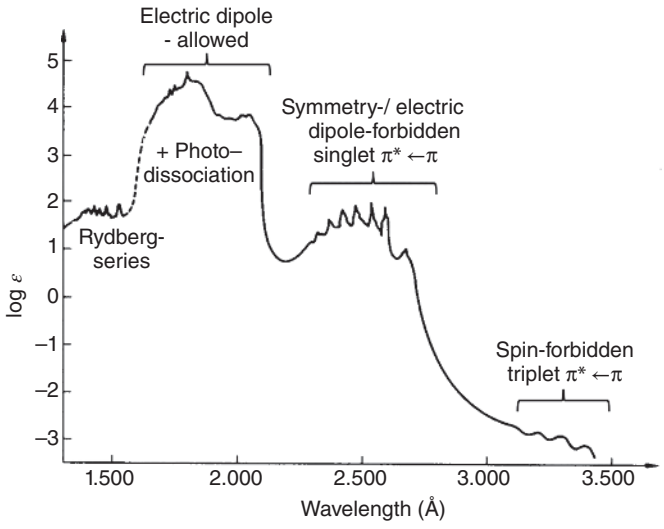

Figure 1.5 Absorption spectrum of benzene, illustrating the dipole transition probabilities according to selection rules. Source: Modified from Barrow (1962).

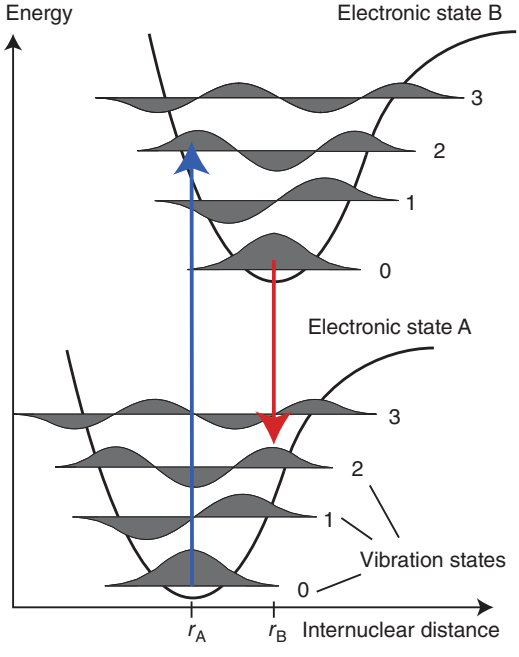

Figure 1.6 Electronic transitions are faster than nuclear motion. The nuclei rearrange after electronic excitation (vertical blue arrow) to the new distance r_B. Transition probability is highest between the vibration states of the greatest waveform overlap, determining the possible final states (Franck-Condon principle). For examples on Franck-Condon controlled vibronic spectrum, see the analysis of the biphenylene REMPI spectrum and other molecules in chapter 2.

Vibronic transitions in turn induce rotational transitions contributing many more absorption lines, according to the selection rules. Comparable to ice skaters, who extend their arms during a pirouette to slow down their spin, the vibration affects molecular rotation.

Complexity further increases for polyatomic molecules. For small molecules, application of the selection rules must consider their whole symmetry,

as the electronic excitation affects the complete structure. Detailed electronic structures are calculated with methods of computational chemistry that are based on several approximations, e.g. Hartree-Fock (*ab initio*), Post-Hartree-Fock (considers electron correlations), or density functional theory. In many applications, a particular group of atoms in the molecule is considered because they show a characteristic absorption feature. These subgroups, called *chromophores*, may occur in different molecules contributing absorption bands of the same wavelength. Basic considerations on a molecule's absorption behavior can often be reduced to the presence of such chromophores and perturbations from other groups in the molecule. A prominent example is the *B*-band of benzene and derivatives originating from $\pi \rightarrow \pi^*$ transitions. Although this *benzenoid* band is forbidden by symmetry for pure electronic states, it is allowed with respect to the overall symmetry of vibronic states. In context of analytical applications, it contributes the intermediate REMPI states giving the aromatic ring structures high REMPI cross sections for e.g., the fourth harmonic of the Nd:YAG laser (266 nm). Comprehensive collections of photoabsorption spectral information can be found in the literature, e.g. Berkowitz (2002). Having regard to the scope on photoionization for analytical mass spectrometry, many structural and spectroscopic details can be omitted here, and in the following, we can focus on specific aspects that have practical implications to mass spectrometry. In chapter 2 the application of REMPI in molecular spectroscopy using tunable lasers is discussed with the help of photoabsorption and ionization spectra of suited interesting molecular systems.

1.3.8 Single-photon Ionization (SPI)

So far, electronic transitions between bound states were treated. Their probabilities at given photon energies and radiation intensities are formally determined by (dipole-) transition matrix elements or more practically by absorption cross sections (ref. Eqs. (1.33, 1.34)) (Berkowitz 2002). Corresponding absorption spectra are often characterized using oscillator strength values (Eq. (1.38)). If an electron is released by the absorption process, the final state has a free electron, allowing continuous values for its energy E_{kin} and momentum $\mathbf{p}_e$ (continuum state). Consequently, SPI is less constrained to structural and electronic properties, and its cross sections show a rather narrow distribution, enabling to use SPI for a universal ionization of molecules (threshold selectivity $Eh\nu \geq IE$), see also Chapter 3 for SPI-MS applications. SPI and possible subsequent fragmentation of a molecule *AB* in the ground vibronic state can be formally written as

$$AB + h\nu \rightarrow [AB^+]' + e^- \tag{1.41}$$

$$[AB^+]' \rightarrow AB^+ \text{ and/or } A + B^+ \tag{1.42}$$

with the quotation mark indicating the excited state. Again, the timescale of the electron ejection process (Eq. (1.41)) is much shorter compared to the relaxation described by Eq. (1.42). Consequently, the electron energy E_{kin} can be measured to probe the energy E_B of the excited state of the molecular ion $[AB^+]'$ via photoelectron spectroscopy (PES) according to $E_{\text{kin}} = h\nu - E_B$. Detailed ionization and fragmentation studies are facilitated by combining MS with PES, ideally in

a single-event coincidence setup, called photoelectron photoion coincidence (PEPICO) spectroscopy (Baer 2000). The special case of $E_{\mathrm{kin}} \simeq 0$ eV ("threshold PEPICO") allows the precise determination of the energy E_B of the molecular ion and has been used to work out the thermochemistry of many gas-phase species (Sztáray et al. 2010).

Allowing multiple charging ($n > 1$) and with the focus on mass spectrometry, Eqs. (1.41) and (1.42) may also be summarized as

$$AB + h\nu \rightarrow [AB^{n+}]' + ne^- \tag{1.43}$$

$$\searrow AB^{n+} \tag{1.44}$$

$$\searrow A^{p+} + B^{q+} \tag{1.45}$$

$$\searrow A^+ + B^- \ (n = 0) \tag{1.46}$$

For chemical analyses using single-photon ionization mass spectrometry (SPI-MS), the case of Eq. (1.44) with $n = 1$ is typically desired, while Eq. (1.45) refers to production of fragment ions of charge p^+ and q^+ and Eq. (1.46) refers to ion-pair production. Ionization energies (*IEs*) of organic molecules reside in the range of 8–12 eV. Because the values of atmosphere gases as N_2, O_2, H_2O, etc. , are higher, they typically do not interfere in SPI-MS analyses. Fragmentation increases with photon energy; thus, the desired photon energy is about 10–15 eV, a region where the ionization efficiency varies strongly and where compact, robust, and intense light sources are rare. Dependent on the analyte molecules, the gap between *IE* and the appearance energies of one or more fragmentation pathways differs widely and molecules may not only be ionized but also undergo direct or metastable fragmentation, see Figure 1.7 for an example.

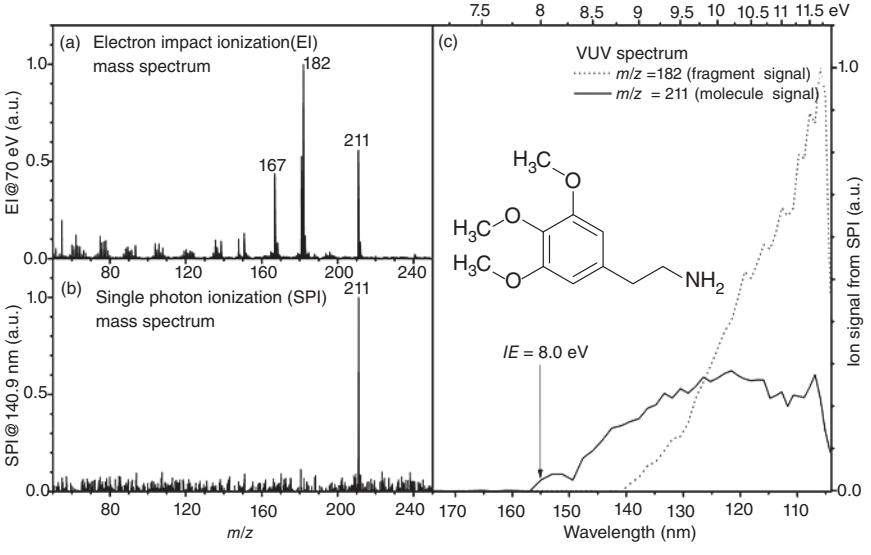

Figure 1.7 Ionization and fragmentation behavior of mescaline. (a) Electron impact ionization with 70 eV electron energy leads to substantial fragmentation, in contrast to (b) single-photon ionization (SPI) with 8.8 eV synchrotron radiation. (c) Fragment-free SPI is possible for a photon energy around 8–9 eV, limiting the choice of VUV light sources for SPI. Source: Kleeblatt et al. (2013). Modified with permission of SAGE.

This behavior is typical for several relevant compounds classes, e.g. for many explosives, drugs of abuse and pharmaceutical active compounds, as well as for the majority of metabolites. For many other compounds, such as alkanes or alkylated aromatic compounds, however, a totally soft ionization by SPI is achieved. Particular high stability is observed for aromatic compounds because the charge is delocalized throughout the whole ring (resonance stabilization) (Edirisinghe et al. 2006; Gunzer et al. 2019). The ionization energy can be obtained with relatively good accuracy by quantum chemical calculations: According to Koopmans' theorem, the vertical *IE* equals the negative energy of the highest occupied molecular orbital (HOMO). The underlying approximation neglects changes of the energy levels through rearrangements upon removal of the electron from the HOMO. Adiabatic values for *IE* can be obtained from the difference of the total energies of the geometry-optimized molecular ground state and the respective ionic state (Gross 2011). In general, smaller homologues of a molecular substance class exhibit higher ionization energies than its larger homologues. For organic compounds, *IE* can also be influenced by substituents, which can either withdraw electron density from the HOMO or push electron density into the HOMO via mesomeric or inductive effects. The highest molecular *IE* values are observed for small inorganic compounds such as *HF* (16.03 eV, highest molecular *IE*), F_2 (15.70 eV), N_2 (15.58 eV), H_2 (15.43 eV), CO_2 (13.78 eV), H_2O (12.62 eV), or O_2 (12.07 eV). Methane has the highest *IE* for a hydrocarbon (12.61 eV). Ionization energies as a function of molecular weight (m/z) for different organic compound classes are shown in Figure 1.8. Generally, the values of *IE* decrease with increasing molecular size within a homologous series. For very large molecules, they hyperbolically approach a value close to the work function of the respective bulk material, see the intersections with the y-axis in Figure 1.8(b). Obviously, there is no apparent size limit in photoionization as demonstrated in studies on large molecules (Akhmetov et al. 2010; Schätti et al. 2017). The *IE* of condensed aromatic compounds are generally lower than the values of aliphatic compounds, as the ionization occurs from the HOMO of the aromatic π-electron system (delocalized). Substitution can induce different effects on *IE*, as illustrated in Figure 1.8: substituents that withdraw electron density from the π-electron system, such as the halogens, fluorine, and chlorine, tend to increase *IE* upon successive substitution of *H*-atoms at the aromatic moieties. On the other hand, substitution by electron-donating groups, such as methyl groups, causes a decrease of *IE* with an increasing degree of substitution.

The second fundamental parameter for SPI is the single-photon ionization cross section σ_{SPI}. From the photon flux φ through the sample volume V (cm^3), the concentration C of molecules ($n\ cm^{-3}$) and the absolute σ_{SPI} value, the ionization rate R_{SPI} (n/s) can be calculated according to

$$R_{SPI} = \sigma_{SPI} \varphi V C \tag{1.47}$$

Experimental values of σ_{SPI} for several homologous or substituted compounds as a function of molecular weight are depicted in Figure 1.9. The measurements have been performed using a gas chromatograph coupled to a mass spectrometer equipped with an electron beam excimer lamp for SPI (Eschner and Zimmermann 2011). For all compounds, a slight increase of the σ_{SPI} values with rising molecular weight is observed. The similarities of SPI cross sections for members

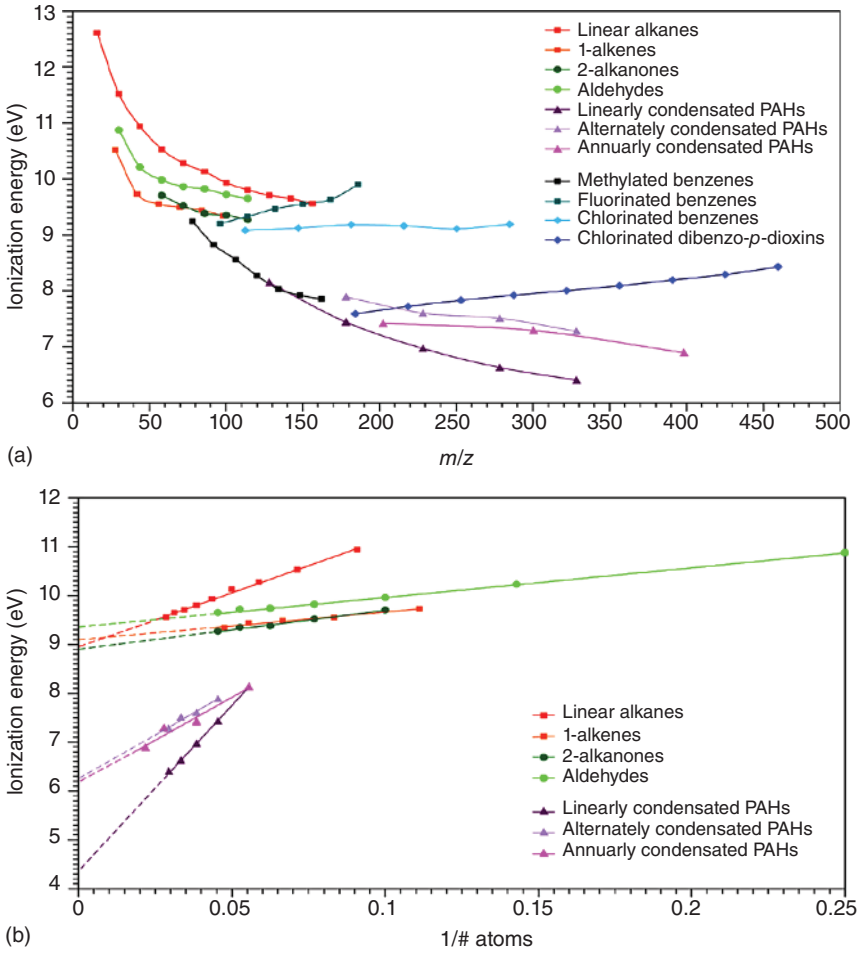

Figure 1.8 Ionization energies plotted against (a) the molecular weight for different homologous organic compounds and (substituted) aromatic hydrocarbons (homologous series for alkanes, 1-alkenes, aldehydes and alkanones; increasing substitution degree from 1-6 for benzene derivatives (for alkylated benzenes: 1-5, from toluene to pentamethylbenzene) and 1-8 for chlrorinated dibenzo-*p*-dioxins; differently condensed rings for polycyclic aromatic hydrocarbons (PAH)). (b) The molecular *IE* values plotted against the inverse number of atoms illustrate their approach toward material's work function (conducting material) or ionization energy (insulators) for large atom numbers. Source: Data from NIST Chemistry Webbook and National Institute of Standard and MD Technology.

within a particular compound class can be used for approximate (semi-) quantification. Note that σ_{SPI} also depends on the spectral shape of the respective light source. For compounds with an *IE* within the emission band, only the fraction of photons exceeding *IE* can contribute to ionization. This results in a relative suppression of the observed σ_{SPI} compared to the compounds with lower *IE*. The effect can be noticed for the n-alkanes as depicted in Figure 1.9(b). Here, the slope of σ_{SPI} of n-alkanes (red) is lower for the smaller homologues ($1/n \gtrapprox 0.02$), exhibiting *IE* values within the lamp's emission band.

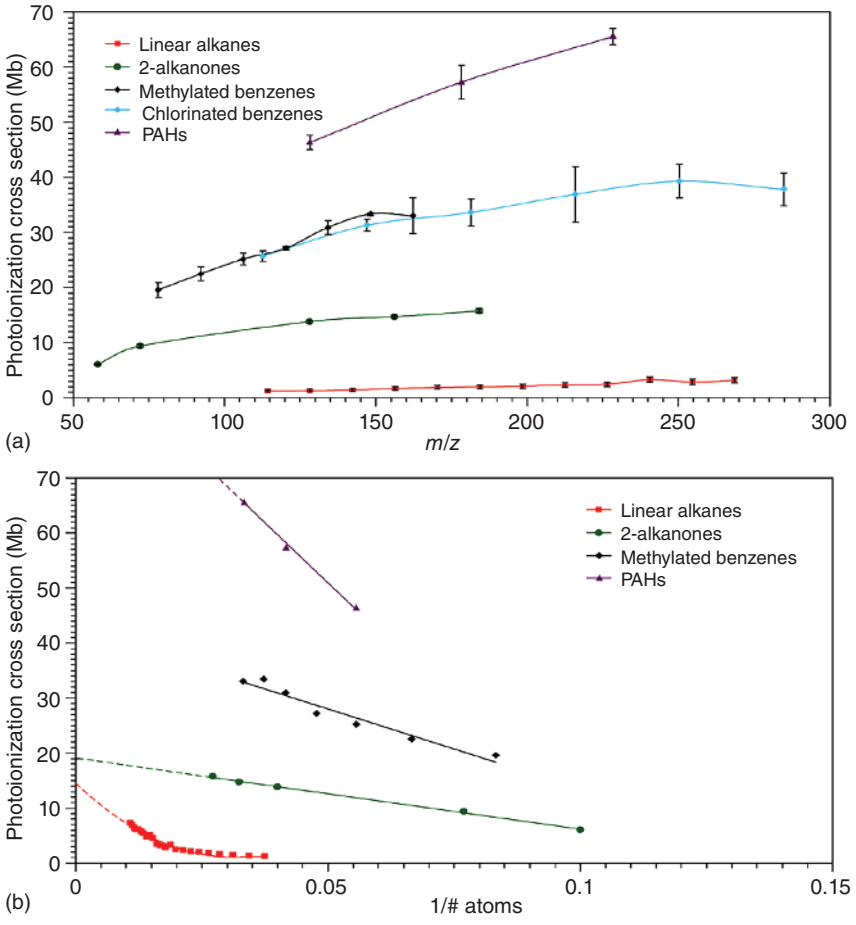

Figure 1.9 Single-photon ionization cross sections σ_{SPI} at 9.8 eV (0.4 eV FWHM) plotted against (a) the molecular weight and (b) the inverse atom number of different compound classes (homologous series for alkanes and alkanones; increasing substitution degree from 1-6 for benzene derivatives, linearly condensed rings for polycyclic aromatic hydrocarbons (PAH): naphthalene, anthracane, tetracene). The flatten of the curve toward smaller linear alkanes is due to their relatively high *IEs*, in particular for the lower molecular weight species (see Figure 1.8). Therefore, only a fraction of the VUV-emission spectrum of the used lamp can be used for the ionization. Source: Data from Eschner and Zimmermann (2011).

If the IE is plotted against the inverse number of atoms (Figure 1.8b) the IE limit for very large molecules can be estimated. For infinitely large molecules this IE converges to the respective solid state material property. In the case of the PAH this correspond to graphite, which is a conducting solid with a work function of 4.7 eV (Rut'kov 2020), or an individual graphene layer with a work function of 4.3 eV (Rut'kov 2020). Polypropylene (PP) in contrary is a model for a fully saturated, insulating solid state polymer, which exhibit a solid state ionisation energy of 8.65 eV (Rajopadhye, 1986). The extended lines for the linearly condensed PAH and the fully saturated linear alkanes in Figure 1.8b hit the x axis (i.e. infinitely large molecule) at the values of 4.4 eV (PAH) and 8.8 eV

(alkanes), showing a very good agreement of estimation and experimental data. With respect to the photoionization of very large molecules it is notable that there was an intense discussion about the question, if larger molecules indeed can be efficiently photoionized (Schlag 1992). It was suggested, that SPI efficiency of larger molecules is decreasing with molecular size due the incensing density of states, which supports the rapid dissipation of energy supplied by photon absorption into internal charge transfer states.

The dissipated energy then cannot be recombined quickly enough for a timely (auto-)ionization. However, already in 1995 single photon ionization of fullerenes and carbon clusters up to 2000 m/z was reported (Becker 1995). Recently, a fs laser desorption SPI-post ionization experiment demonstrated that efficient SPI of complex polypeptides with more 20.000 m/z is possible (Schätti 2018).

Generally, cross sections for SPI are lower than the values of the standard ionization via electron impact (EI). In contrast to the rather weak dipole interaction with the light field in SPI, the electron's de Broglie wavelength in EI (70 eV, $\approx$ 1.5 pm) matches the typical bond lengths in organic molecules. Thus, the energy transfer to the analyte and ionization efficiency is maximized. Also, the cross-sectional variance of about 10 for different compound classes is rather low for the universal ionization method EI (Adam and Zimmermann 2007). However, despite lower cross sections, respective sensitivity, SPI features ionization with very low fragmentation and produces no interfering signals from the carrier gas (higher IE), rendering it an ideal method for complex organic mixtures. Such practical considerations and the unique features of (resonance-enhanced) multiphoton ionization will be discussed in Chapters 2, 4 and 11 of this book.

References

Adam, T. and Zimmermann, R. (2007). Determination of single photon ionization cross sections for quantitative analysis of complex organic mixtures. *Anal. Bioanal. Chem.* 389 (6): 1941–1951.

Akhmetov, A., Moore, J.F., Gasper, G.L. et al. (2010). Laser desorption postionization for imaging MS of biological material. *J. Mass Spectrom.* 45 (2): 137–145.

Baer, T. (2000). Ion dissociation dynamics and thermochemistry by photoelectron photoion coincidence (PEPICO) spectroscopy. *Int. J. Mass Spectrom.* 200 (100): 443–457.

Barrow, G.M. (1962). *Introduction to Molecular Spectroscopy*. McGraw Hill.

Baumert, T. and Gerber, G. (1997). Molecules in intense femtosecond laser fields. *Phys. Scr.* T72: 53–68.

Becker, C.H. and Wu, K.J. (1995) On the photoionization of large molecules. *J. Am. Soc. Mass. Spectrom.* 6: 883–888.

Berkowitz, J. (2002). *Atomic and Molecular Photoabsorption. Absolute Total Cross Sections*. London: Academic Press.

Edirisinghe, P.D., Moore, J.F., Calaway, W.F. et al. (2006). Vacuum ultraviolet postionization of aromatic groups covalently bound to peptides. *Anal. Chem.* 78 (16): 5876–5883.

Eschner, M. and Zimmermann, R. (2011). Determination of photoionization cross-sections of different organic molecules using gas chromatography coupled to single-photon ionization (SPI) time-of-flight mass spectrometry (TOF-MS) with an electron beam pumped rare gas excimer light source (EBEL): influence of molecular structure and analytical implications. *Appl. Spectrosc.* 65: 806–816.

Gross, J.H. (2011). *Mass Spectrometry*. Springer.

Gunzer, F., Krüger, S., and Grotemeyer, J.H.C. (2019). Photoionization and photofragmentation in mass spectrometry with visible and UV lasers. *Mass Spectrom. Rev.* 38 (2): 202–217.

Kleeblatt, J., Ehlert, S., Hölzer, J. et al. (2013). Investigation of the photoionization properties of pharmaceutically relevant substances by resonance-enhanced multiphoton ionization spectroscopy and single-photon ionization spectroscopy using synchrotron radiation. *Appl. Spectrosc.* 67 (8): 860–872.

National Institute of Standard and MD Technology NIST Chemistry WebBook. Standard reference database. Gaithersburg. http://webbook.nist.gov/chemistry.

Rajopadhye, N.R. and Bhorarkar, S.V. (1986). Ionization potential and work function measurements of PP, PET and FEP using low-energy electron beam. *J. Mat. Sci. Lett*. 5: 603–605.

Rut'kov, E.V., Afanas'eva, E.Y., and Gall, N.R., (2020). Graphene and graphite work function depending on layer number on Re. *Diamond Rel. Mat.* 101: 107576.

Schätti, J., Rieser, P., Sezer, U., et al. (2018). Pushing the mass limit for intact launch and photoionization of large neutral biopolymers. *Commun. Chem.* 1: 93. https://doi.org/10.1038/s42004-018-0095-y.

Schätti, J., Sezer, U., Pedalino, S. et al. (2017). Tailoring the volatility and stability of oligopeptides. *J. Mass Spectrom.* 52 (8): 550–556.

Schlag, E.W., Grotemeyer, J., and Levine, R.D. (1992). Do large molecules ionize? *Chem. Phys. Lett.* 190: 521–527.

Sztáray, B., Bodi, A., and Baer, T. (2010). Modeling unimolecular reactions in photoelectron photoion coincidence experiments. *J. Mass Spectrom.* 45 (11): 1233–1245.